Dual-Material 3D-Printed Intestinal Model Devices with Integrated Villi-like Scaffolds

Taebnia, Nayere; Zhang, Rujing; Kromann, Emil B; Dolatshahi-Pirouz, Alireza; Andresen, Thomas L; Larsen, Niels B.

Published in:
ACS Applied Materials and Interfaces

Link to article, DOI:
10.1021/acsami.1c22185

Publication date:
2021

Document Version
Peer reviewed version

Dual-material 3D printed intestinal model devices with integrated villi-like scaffolds

Nayere Taebnia[‡] Rujing Zhang[‡] , Emil B. Kromann, Alireza Dolatshahi-Pirouz, Thomas L. Andresen,[*] and Niels B. Larsen[*]

Center for Intestinal Absorption and Transport of Biopharmaceuticals, Department of Health Technology, Technical University of Denmark, DK-2800, Kgs. Lyngby, Denmark.

Keywords: 3D Tissue models, Intestinal barrier, Villi, Multi-material 3D printing, Stereolithography, Hydrogels.

Abstract

In vitro small intestinal models aim to mimic the *in vivo* intestinal function and structure, including the villi architecture of the native tissue. Accurate models in a scalable format are in great demand to advance, for example, the development of orally administered pharmaceutical products. Widely used planar intestinal cell monolayers for compound screening applications fail to recapitulate the three-dimensional (3D) microstructural characteristics of the intestinal villi arrays. This study employs stereolithographic 3D printing to manufacture biocompatible hydrogel-based scaffolds with villi-like micropillar arrays of tunable dimensions in poly(ethylene glycol) diacrylates (PEGDAs). The resulting 3D-printed microstructures are demonstrated to support month-long culture and induce apicobasal polarization of Caco-2 epithelial cell layers along the villus axis,

similar to the native intestinal microenvironment. Transport analysis requires confinement of compound transport to the epithelial cell layer within a compound diffusion-closed reservoir compartment. We meet this challenge by sequential printing of PEGDAs of different molecular weights into a monolithic device, where a diffusion-open villus-structured hydrogel bottom supports cell culture and mass transport within the confines of a diffusion-closed solid wall. As a functional demonstrator of this scalable dual-material 3D micromanufacturing technology, we show that Caco-2 cells seeded in villi-wells form a tight epithelial barrier covering the villi-like micropillars, and that compound-induced challenges to the barrier integrity can be monitored by standard high-throughput analysis tools (fluorescent tracer diffusion and transepithelial electrical resistance, TEER).

Introduction

Orally administered drugs are mainly absorbed in the small intestine,[1] calling for reliable *in vitro* intestinal models as a tool to engineer drug uptake and assess toxicity.[2,3] Existing models, scalable to industrially relevant numbers, have been restricted to two-dimensional (2D) monolayers of a human colorectal carcinoma cell line (Caco-2) cultured on standard Transwell inserts, i.e., microtiter plate inserts with a microporous membrane allowing for diffusive transport between separate liquid compartments.[4,5] While the simple and robust Transwell models have provided important biological insight, such 2D models fail to recapitulate the complex 3D microenvironment of the small intestine with associated limited predictive value of drug uptake and transport.[4,6] The small intestine luminal surface presents a dense array of “crypt-villus” units. Villi are finger-like protrusions maximizing the surface area for absorption, while crypts are well-

like invaginations at the base of each villus accommodating intestinal stem cells. The function of the small intestine is maintained by constant renewal of the epithelium through guided migration and differentiation of the intestinal stem cells along the crypt-villus axis.[7,8] Hence, it is of significant importance to include such microarchitectures to create more physiologically relevant *in vitro* intestinal models.

To address the limitations of conventional 2D models, more advanced culture systems have recently been developed to study the intestinal epithelium.[9–11] Primary intestinal stem cells isolated from mouse or human gut specimens have been successfully cultured *in vitro* using extracellular matrix such as Matrigel to form organoids exhibiting distinctive crypt- and villi-like domains.[12–14] Although these 3D models capture the intrinsic heterogeneity of the intestinal tissue, their cystic architecture complicates luminal access and reduces their applicability for compound screening. Alternatively, microfabrication techniques have been utilized to engineer 3D scaffolds that better mimic the topography of intestinal crypts and villi.[15–29] These micro-patterned scaffolds were seeded with intestinal cells, most often intestinal cell lines such as Caco-2 being a widely used, easily accessible, cost-effective, and robust cell model, and used in combination with standard Transwell inserts to allow for assays with quantitative readouts such as transepithelial electrical resistance (TEER)[30] and permeability testing. However, these platforms are mostly engineered through time-consuming and labor-intensive multi-step molding processes. In addition, extra efforts as well as specialized equipment dedication are required to ensure tight attachment to the Transwell insert so that mass transport is restricted to the cell-coated scaffold.[16,17,19,23–25] The most widely used materials for molding intestinal scaffolds are collagen[15–17,24,29] and poly(lactic-co-glycolic acid) (PLGA).[23,25] Collagen promotes cell adhesion and growth, but its application as an *in vitro* 3D scaffold for extended culture times is challenged by its short-term loss of structural

fidelity and stability. Moreover, collagen hydrogels have been reported to reduce the passage of some hydrophobic drug molecules due to their absorption by the collagen network.[16] PLGA is more mechanically stable but requires the engineering of porosity to enable diffusive mass transport.[23] Several "gut-on-a-chip" microfluidic platforms developed in the past decade have been shown to mimic important aspects of the physiologically dynamic environment *in vivo* such as fluidic shear stress and peristaltic motions.[31–38] Recently, microfluidics and planar villi-like structures laser-cut in hydrogel sheets were elegantly combined with culture of mouse intestinal stem cells to recapitulate important aspects of cell-fate patterning along the crypt-villus axis.[39] However, many of these microfluidic systems are engineered using soft lithography in polydimethylsiloxane (PDMS), which does not allow for aqueous compound transport and provides limited topological design freedom, and typically requires multiple processing steps for manufacture of a final device. Another major challenge in these microfluidic platforms is to perform industry-standard TEER analysis, which has either not been implemented or requires complicated setups.[32,34,40–42] Despite the listed limitations, these advanced models have demonstrated the favorable influence of 3D intestine-like microenvironments on cell functions, including proliferation, differentiation and polarization.

In recent years, 3D printing (additive manufacturing) has emerged as a powerful approach to create complex 3D constructs.[43] High resolution 3D printing allows for the direct manufacture of free-form features, with or without overhangs, including shapes mimicking the slightly tapered villi of the small intestinal wall. Additionally, this technique enables accurate definition of the interface in 3D when combining overlaying segments of two materials, which is highly challenging using conventional multi-step molding processes. Laser scanning stereolithography (SLA) of a 3D poly(ethylene glycol) (PEG) based hydrogel scaffold reproducing intestinal epithelium topography

has been reported.[44] However, the serial voxel-by-voxel fabrication process characteristic of fine-spot laser scanning resulted in extended manufacturing times of about 12 h. Additionally, the reported single-material scaffold cannot function as a self-contained system, hence limiting higher throughput applications and quantitative analysis of barrier integrity.[44] Projection SLA, as opposed to laser scanning SLA, offers larger volumetric throughput of complex structures enabled by parallel whole-layer exposure.[45,46] SLA is based on light-induced solidification of a liquid resin, most commonly by radical or cationic photopolymerization, which usually results in single-material constructs. A single material supporting cell culture and mass transport, exemplified by a hydrogel with cell adhesive motifs, is ideal for intestinal scaffolds. However, manufacturing of a self-contained device for compartmentalized compound transport analysis calls for spatially selective diffusion properties provided by co-structuring of different materials. Dual-material SLA by intermediate resin change has been reported previously [47–52] but not for engineering local diffusive properties in cell culture systems.

Our focus is to address the aforementioned challenges in establishing a robust and easily accessible analysis platform based on diffusion-tunable, yet mechanically stable and topographically accurate, *in vitro* models capable of supporting intestinal enterocyte culture, and to enable quantitative characterization of barrier integrity in a reproducible and scalable format by taking advantage of projection SLA. We hypothesize that chemically similar monomeric starting materials can be combined to form mechanically and dimensionally stable monolithic entities with spatially variable physiochemical properties, such as aqueous compound diffusion, after cross-linking during 3D printing. We report on the fabrication of SLA printed dual-material 3D cell culture scaffolds, termed villi-wells, which encompasses villi-like diffusion-open micropillar arrays at the bottom, enclosed by a diffusion-closed wall, as micro-topographically structured

analogues of Transwell inserts (Scheme 1a). To this end, poly(ethylene glycol) diacrylates (PEGDA) of two different molecular weights are utilized to print each part of the dual material structures. The bottom part, containing the villi-like micropillars, is composed of a diffusion-open hydrogel material made from a medium molecular weight PEGDA and supplemented with a cell adhesive protein to support cell culture. The villi-well wall is, on the other hand, made of crosslinked low molecular weight PEGDA, a diffusion-closed non-swellable material. This confines diffusive transport of ions, measured by TEER, and other aqueous compounds to occur through the bottom hydrogel part (Scheme 1a). We explore the achievable design complexity and detail by varying the inter-pillar spacing, structurally characterizing the resulting printed devices, and evaluating the effect of villi-like structures on the organization and transport properties of subsequently cultured epithelial monolayers.

Materials and methods

Synthesis of Gelatin methacrylate (GelMA)

GelMA was synthesized according to a previously reported method.[53] Briefly, 10 g of gelatin (from porcine skin, Type A, gel strength ~300 g Bloom, Sigma Aldrich) was gradually dissolved into 100 mL of pre-warmed Dulbecco's phosphate-buffered saline (DPBS, Sigma Aldrich) at 50 °C under continuous stirring. After dissolution, 5.8 mL methacrylic anhydride (Sigma Aldrich) was added and the mixture was vigorously stirred for 1 h. Once the reaction was completed the mixture was centrifuged, and the obtained supernatant was diluted and dialyzed against Milli-Q water (Millipore, >18.2 MOhm cm) for 7-10 days to remove unreacted reagents using a dialysis membrane (cutoff 12-14 kDa) with the water being exchanged every day. Finally, the product was

lyophilized and stored at -20 °C. The degree of methacrylation was determined to be ~60% by ^{1}H NMR, calculated from the integrated area of the lysine ε-methylene peak at 2.92 ppm for unmodified gelatin and for GelMA.

3D printing of the dual-material villi-wells

Dual-material scaffolds were fabricated using a custom-built projection based stereolithography printer. The printer and its characteristics have been described in our previous work.[54,55] Briefly, collimated light from a 365-nm high-power LED (LZ1-00UV00, Ledengin) impinges on a Digital Mirror Device (10.8 μm pixel pitch, DLP9500 UV, Texas Instruments, DMD), and the resulting image is projected 1:1 onto the bottom of a vat containing the printing resin (power density 10.9 mW cm^{-2}) (Scheme 1b). Cover glasses (22 × 22 × 0.4 mm^3, Thermo Scientific Menzel Haemacytometer Coverslip), functioning as print substrates, were silanized with 3-(trimethoxysilyl)propyl methacrylate (Sigma-Aldrich)[54] to promote adhesion of prints to the glass support. Non-adhesive fluorinated ethylene propylene (FEP) foil (DuPont Fluoroplastic Film), applied to the vat bottom, facilitated smooth release of each printed layer from the vat. 3D models of the villi-wells were designed using Inventor 2018 (Autodesk) and subsequently sliced into a series of digital masks with a slicing thickness of either 20 or 50 μm, for the bottom hydrogel and the wall, respectively, using the open-source slicer software Slic3r. Dual-material printing was carried out in two steps. In the first step, the resin consisted of an aqueous solution of 200 mg mL^{-1} poly(ethylene glycol) diacrylate (M_n 700 g mol^{-1}, PEGDA700, Sigma-Aldrich), 20 mg mL^{-1} GelMA, 5 mg mL^{-1} lithium phenyl-2,4,6-trimethylbenzoylphosphinate (LAP, Sigma-Aldrich, photoinitiator) and 12 mg mL^{-1} Quinoline Yellow (QY, Sigma-Aldrich, photoabsorber), optimized

for printing resolution in our former publication.[54] For the prints used for structural analysis by confocal fluorescence microscopy, the aqueous resin was supplemented with 20 µg mL^{-1} fluorescent beads (200 nm, carboxylate-modified microspheres, yellow-green fluorescent 505/515, FluoSpheres™, Thermo Fisher Scientific). The first few layers (corresponding to ~200 µm thickness) were exposed for 4 s at a reduced step height of either 5 or 10 µm to ensure proper attachment of the polymer to the glass. Remaining layers were exposed for 3 s at a step height of 20 µm. After printing the diffusion-open bottom, the built-stage with the mounted structure was removed from the printer and briefly rinsed in DI water. Surplus water was immediately removed by lens tissue paper. In the second step, the aqueous resin in the vat was replaced by pure poly(ethylene glycol) diacrylate (M_n 250 g mol^{-1}, Sigma-Aldrich, PEGDA250) containing 4 mg mL^{-1} phenylbis(2,4,6-trimethylbenzoyl)phosphine oxide (Irgacure 819, Sigma-Aldrich, photoinitiator, soluble in PEGDA250) and 1 mg mL^{-1} Avobenzone (Sigma-Aldrich, photoabsorber, soluble in PEGDA250) (see the Supporting Information for details on optimizing the print formulation and for rheological properties of the two resins). The print substrate with the printed PEGDA700/GelMA part was moved to the last position of the first printing process. The first few layers (corresponding to ~150 µm thickness) were exposed for 4 s at a reduced step height of 25 µm to ensure proper attachment, and the remaining part was exposed for 3 s for each layer at a step height of 50 µm. The manufacturing time per villi-well was 35 minutes (two devices produced in parallel in 70 minutes). The resulting dual-material villi-well was thoroughly rinsed in ethanol to remove remaining resin and subsequently immersed in Milli-Q water. The prints remained immersed for a couple of days to leach out remaining reagents, mostly from the diffusion-open hydrogel compartment, as well as to reach its equilibrium swelling. Finally, the still-immersed villi-wells were post-cured for 12 h by UV-A illumination (365 nm, 4.5 mW cm^{-2},

CUREbox™ CB-4230, Wicked Engineering). The structural accuracy was quantified from tiled confocal stacks acquired on the entire area of two villi wells for each villi spacing, for a total of >100 villi analyzed for each spacing. The height, base diameter, and interpillar spacing were measured for all micropillars using Zeiss Zen 2012 Black Edition software after correcting for the effect of the refractive index of water on the measured heights.

Swelling study

Solid single-material rectangular blocks (10 × 10 × 3.5 mm^3) were printed on cover glasses in PEGDA250, PEGDA700 (without added GelMA), and PEGDA700/GelMA, using the resin formulations and procedure described above. Immediately after printing, each sample was removed from the cover glass by a scalpel. The surplus resin on the surfaces was removed by tissue paper, and the sample weight was measured. The samples were then immersed in DI water, and their weight was monitored periodically until reaching equilibrium. The swollen samples were eventually lyophilized to obtain the dry weight for calculating the mass swelling ratio (q), defined as $q = M_s/M_d$ with M_s and M_d being the mass of the swollen and the dry structures, respectively.

Mechanical characterization

Solid single-material cylinders of 6 mm diameter and 5 mm height were printed using the three resin formulations described above. The printed cylinders were immersed in DI water to reach their equilibrium degree of swelling. The still-wet samples underwent a compression test using a mechanical tester (Instron 5967, UK) equipped with a 500 N load cell, at a compression rate of 0.5

mm min^{-1} until breakage. The stress-strain data was analyzed using neo-Hookean rubber elastic theory that predicts a linear dependence of the stress on λ-λ^{-2} (λ being the extension ratio).[56]

Cell line maintenance

Human colon adenocarcinoma (Caco-2) cells (Sigma-Aldrich) were cultured in Minimum Essential Medium Eagle (MEM, Sigma-Aldrich) supplemented with 10% v/v fetal bovine serum (FBS, Sigma-Aldrich), 1% v/v L-glutamine solution (200 mM, Sigma Aldrich), 1% v/v MEM non-essential amino acid solution (NEAA, Sigma-Aldrich) and 1% v/v penicillin-streptomycin (P/S, Sigma-Aldrich). Cells were cultivated in T75 culture flasks at 37 °C and 5% CO2 with medium renewal every 2-3 days and passaged weekly. For all experiments, Caco-2 cells were used between passage 50 and 65.

Cytotoxicity Assay for PEGDA 250

Bowl structures ($Ø_{inner}$ 4.5 mm, $Ø_{outer}$ 6.5 mm, 0.6 mm thick bottom, 3.1 mm overall height) were printed using non-aqueous resin PEGDA 250 and subsequently post-cured for 12 h by UV-A illumination (365 nm, 4.5 mW cm^{-2}, CUREbox™ CB-4230, Wicked Engineering). To promote cell adhesion, 30 µL aqueous solution of 20 mg mL^{-1} GelMA and 5 mg mL^{-1} LAP was added to each bowl, followed by 10 min of UV-A illumination. The reaction mixture was removed, and the structures were washed with DI water 3 times before being immersed in serum-free medium (MEM) supplemented with 2% v/v P/S. The printed bowls were then sterilized by 20 min exposure of UV-C irradiation (254 nm, UV sterilization cabinet, Cleaver Scientific) in a laminar flow bench.

Prior to cell seeding, the surface of the sterile bowls was further incubated with 10 μg mL^{-1} fibronectin (fibronectin bovine plasma, Sigma-Aldrich) at 4 °C overnight. Caco-2 cells were harvested from the culture flask at 75% confluency using 0.5% trypsin in DPBS/EDTA (Sigma-Aldrich) and seeded in each printed bowl at 5×10^4 cells cm^{-2} and cultured at 37 °C in 5% CO_2 for 1, 4 and 7 days, respectively. Cells were then stained with calcein-AM (2 μg mL^{-1}, Invitrogen) and propidium iodide (PI, 2 μg mL^{-1}, Sigma-Aldrich) for 1 h. Each sample was characterized by confocal laser scanning microscopy (LSM 700, Zeiss).

Cell culture in villi-wells

Prior to cell seeding, printed scaffolds were submerged in serum-free medium (MEM) supplemented with 2% v/v antibiotic and sterilized by 20 min exposure of UV-C irradiation (254 nm, UV sterilization cabinet, Cleaver Scientific) inside a laminar flow bench. The surface of the sterile villi-wells was then incubated with 10 μg mL^{-1} fibronectin (fibronectin bovine plasma, Sigma-Aldrich) at 4 °C overnight. Caco-2 cells were harvested from the culture flask at 75% confluency, using 0.5% trypsin in DPBS/EDTA (Sigma-Aldrich), and seeded onto the villi-wells at 6.4×10^4 cells per printed well. The villi-wells had previously been placed into either Transwell inserts (24 well, Corning Transwell, 0.4 μm pore size) or 6-well plates, depending on the intended experiment. Cells were cultured for up to 45 days, with the medium being exchanged every 2-3 days for both Transwell inserts (100 μL for apical side and 800 μL for basal side) and 6-well plates. The Transwell-fitted samples were utilized to assess the barrier integrity, while cells in 6-well plates were used for either live/dead staining (2 μg mL^{-1} calcein-AM and 2 μg mL^{-1} propidium iodide for 1 h) or immunostaining.

Barrier integrity assay

To evaluate the integrity of the epithelial barrier formed on the 3D structure of the villi-wells, standard protocols were employed. The transepithelial electrical resistance (TEER) between the two compartments was monitored every 5 days using an EVOM2 epithelial voltmeter equipped with EndOhm culture cup (World Precision Instrument). The resistance of the blank scaffold without cells was subtracted from the measured resistance values, which were then normalized by multiplying with the developed surface area (ohm cm^2). The surface area for culture was defined as the inner-well area of the hydrogel bottom including villi-like micropillars and calculated using Autodesk Inventor 2018 (Table S1).

On day 42 of culture (when the TEER values reached a plateau in the villi-wells), the barrier integrity was further evaluated using TRITC-dextran (4.4 kDa, Sigma-Aldrich) as a model diffusing species. Medium was replaced at the basal side and 100 µl of TRITC-dextran solution (0.5 mg mL^{-1} in medium) was added to the apical side. Cell-free villi-wells of the same geometries were analyzed as a control to ensure that the hydrogel itself does not measurably affect the permeability. After 15 and 60 minutes, 100 µL aliquots were collected from the basolateral side and replaced with fresh medium. The fluorescence intensity of the retrieved samples was measured using a microplate reader (Tecan Spark 20M) at 547 nm excitation and 572 nm emission. Drug-induced loss of barrier integrity was investigated by introducing 100 µL of TRITC-dextran solution (0.5 mg mL^{-1} medium) containing 100 µM staurosporine to the apical side following the replacement of the basal medium with fresh medium. At each time point, 100 µL aliquots were sampled and replaced from the basal side, followed by analysis of their fluorescence intensity as

described above. Throughout the experiment, cells were incubated at 37 °C. All experiments were done with four replicates.

Immunostaining

After 10, 21 or 45 days of culture, cells were rinsed with DPBS, fixed in 4% paraformaldehyde solution for 20 min at room temperature, and washed twice for 5 min with DPBS. After washing, cells were permeabilized with 0.3% Triton X-100 (Sigma-Aldrich) for 10 min. The samples were then washed with DPBS and incubated with blocking buffer (3% BSA + 0.1% Tween 20 in DPBS, Sigma-Aldrich) for 45 min. Cells were again washed with DPBS and subsequently incubated with the primary antibodies of interest (Rabbit anti-ZO-1, Invitrogen #617300, 1:125 or Mouse anti-Ezrin, BD Transduction #610602, 1:50) for 60 min at room temperature, washed three times, incubated with secondary antibodies (Goat-anti-rabbit AlexaFluor 488, Thermo Fisher Scientific #A11008, 1:200, or Goat-anti-mouse AlexaFluor 488, Thermo Fisher Scientific #A11001, 1:200) for 30 min and washed three times with DPBS. Finally, all samples were incubated with 7-Aminoactinomycin (7-AAD, 2 μg mL^{-1}, Thermo Fisher Scientific) for 30 min to stain the nuclei prior to imaging.

Image acquisition and analysis

Images of printed scaffolds were captured using a stereo microscope (Motic SMZ-168). Brightfield images of cell cultures in villi-wells were recorded using phase contrast microscopy (Primovert, Zeiss). Confocal images were acquired on an upright Zeiss LSM 700 confocal laser

scanning microscope using excitation at 488 and/or 555 nm. The vertical axis of the acquired confocal z-stack images was corrected for the refractive index of the culture medium using the microscope software package (Zeiss Zen 2012 Black edition). Two-photon fluorescence imaging was performed on a custom-made upright microscope[57] equipped with a femtosecond laser adjustable from 660 to 1320 nm (Chameleon Discovery, Coherent) and a 25X 1.0 NA water immersion objective (XLPLN25XSVMP2, Olympus) using excitation at 980 and 1100 nm. Z-stack images were recorded at a step height of 2 μm. Composite microscopy images were generated using Fiji by combining different fluorescence channels.

Statistical analysis

All quantifications are presented as mean ± standard deviation, unless stated otherwise. Statistical analysis was performed using GraphPad Prism 7 software (San Diego). A difference between groups was considered statistically significant if $p < 0.05$. Data sets were compared through one-way analysis of variance, followed by Tukey's post hoc test.

Results and discussion

Sequential stereolithography can combine contrasting diffusive and mechanical properties in a monolithic device

Stereolithographic 3D printing offers high spatial detail but with limited possibilities for combining multiple materials within a print, which is needed for the targeted application. We

overcome this limitation by first printing a device part in a diffusion-open hydrogel material followed by printing another device part in a diffusion-closed hydrophobic material to produce contrasting diffusive properties in a monolithic device (Figure 1a). Successful combination of different materials in stereolithography requires covalent bonding between the material layers by compatible crosslinking chemistry. Equally important, the second resin should not cause significant changes in the volume of the first printed material, since contraction or expansion will lead to changes in layer spacing and resulting poor or failing cohesion between layers in the stereolithographic process. The hydrogel part of our device is printed from resin I, an aqueous resin[54] containing medium molecular weight PEGDA monomers (M_n 700 g mol^{-1}, 200 mg mL^{-1}, PEGDA700), photoinitiator (LAP) and photoabsorber (QY). A small amount of gelatin methacrylate is incorporated into the prepolymer mixture for the cell culture studies to provide arginine-glycine-aspartic acid (RGD) sequences that promote cell attachment. Resin II for the diffusion-closed part consists of undiluted low molecular weight PEGDA (M_n 250 g mol^{-1}, PEGDA250) with dissolved photoinitiator (Irgacure 819) and photoabsorber (avobenzone).

We initially tested the resulting diffusive properties using large 3D printed well structures consisting of either pure PEGDA250 or PEGDA250 walls with a bottom of PEGDA700. The dual-material printed wells demonstrated selective permeability towards water-soluble small molecules when immersed in aqueous solutions of a blue food dye (Brilliant Blue FCF, Mallard Ferriere, France). After incubation for 2 h, the bottom compartment was completely infiltrated by the dye while the PEGDA250 wall remained pristine in color (Figure 1b). Compressive mechanical testing and analysis by neo-Hookean theory on 3D printed cylinders of pure PEGDA250, pure PEGDA700, or PEGDA700 with added GelMA showed a 100-fold higher shear modulus (G~58 MPa) of PEGDA250 compared to that of PEGDA700 and PEGDA700+GelMA, both having shear

moduli of G~0.5 MPa (Figure1c). Water swelling analysis of 3D printed material cubes using the same resin compositions found that PEGDA250-based prints show very little swelling, in agreement with the observations of the food dye exposure, while PEGDA700-containing prints exhibit slight post-printing swelling in the first hour after printing until reaching equilibrium (Figure 1d). It should be noted that the change in mass swelling ratio from the freshly printed state to the equilibrium swelling state differs by no more than ~10% (~3% in linear dimension) between the PEGDA250 and the PEGDA700 (without or with added GelMA). This implies that the interface between the PEGDA250 and the compliant PEGD700-based materials only has to accommodate a small interfacial stress at all times. Unreacted leachable acrylates may induce significant cytotoxicity. Our previous work showed that PEGDA700-containing prints are non-cytotoxic[54]. We confirmed a similarly negligible cytotoxicity of PEGDA250-based prints using Caco-2 cells cultured on the planar bottom of test wells printed in PEGDA250 only (Figure S3b).

TEER measurements quantitatively assessed the ion permeability of printed wells using single-material and dual-material resin formulations (Figure 1e). Wells printed solely in PEGDA250 exhibited a high areal resistance, while wells printed in PEGDA700 (with or without added GelMA) or using the dual-material sequence showed similar areal resistance to that of empty Transwells. These results confirm that resin II (PEGDA250) effectively restricts ion transport, thereby enabling reliable TEER measurement through the PEGDA700-based bottom in dual-material prints.

Sequential stereolithography offers stable 3D features at microphysiological detail level

First, the bottom part with a dense array of villi-like micropillars was printed to a total thickness of 0.9 mm using resin I (aqueous PEGDA700 and GelMA). The outer diameter of villi-wells (6.5 mm) was designed to fit into commercial Transwell insert for 24-well plates, and the topography of the micropillars was designed to closely recapitulate the architecture of the human small intestine epithelium. Each micropillar mimicking a single villus was 500 μm in height, with a diameter of 350 μm at the base, and a spherical cap of diameter 300 μm and height 100 μm at the micropillar apex. Varied micropillar spacings, 60, 120, and 180 μm, were used to explore the potential effect of villi density on cell function and proliferation, with smaller spacings offering a better geometric representation of the human small intestinal villi but also limiting diffusive transport of oxygen and nutrients to the cells located in the inter-pillar recesses (Figure 2a). To ease the release of printed wells from the cover glasses and subsequent transfer to Transwell inserts, an array of rectangular blocks ($0.8 \times 0.8 \times 1.0$ mm^3) was included underneath the well bottom as a support structure which could later be removed by a scalpel.

Second, a matching wall of 6.1 mm in height and 1.0 mm in thickness was printed on top of the printed hydrogel structure using resin II (non-aqueous PEGDA250) to produce a self-contained Transwell-like system. The dimension of the wall was designed to match that of the EndOhm electrode used for TEER measurement. The printed stiff PEGDA250 wall, compared to the compliant hydrogel bottom part (Figure 1c) greatly eases the handling of printed scaffolds using common lab tweezers. Water-filled PEGDA700/GelMA hydrogels de-swell in undiluted PEGDA250 and consequently shrink to some extent. However, this shrinkage is reversible after immersion in water (Figure S2c). Transmitted light and fluorescence microscopy analysis confirmed that the delicate villi-like micropillar structures survive the de-swelling/swelling cycle during the two-step printing process. Figure 2b,c shows that the dimensions of the micropillars

(height and diameter) as well as the interpillar spacing closely match the design dimensions. Examples of the tiled confocal microscopy stacks used for the dimensional analysis are shown in Figure S4. Macroscopically, the interface between the two parts also remains largely intact with negligible delamination (Figure S2d). Stability studies showed that the interface of the two compartments and the micropillars maintain their stability even after a year of storage in water (Figure S2c). Degradation studies of test blocks of PEGDA700/GelMA immersed in complete culture medium for the maximum used culture time of 45 days also show as small relative weight loss (3.7±0.4%) and decrease in shear modulus (Figure S3b). Jointly, these results shows that neither of the two printed materials undergo significant post-printing swelling or degradation, and therefore present mechanically and chemically stable structures. These results collectively demonstrate that the initially printed hydrogel network withstands the temporary de-swelling in PEGDATorr250 during the second step of the printing. Swelling reversibility is also enabled by the short printing times involved (each step lasting 30 min for printing two wells in parallel), whereas slower manufacturing processes would result in more extensive de-swelling.

Protein-modified villi-wells support long-term intestinal cell culture

Due to the lack of protein affinity of PEG-based hydrogels, the polymeric networks were further functionalized with extracellular matrix proteins and protein products to support cell adhesion and growth.[58] GelMA was incorporated into the resin I prepolymer solution to covalently anchor molecular binding sites for both cells and cell adhesive proteins in the hydrogel compartment of the villi-wells. Printed constructs were then coated with fibronectin, by physical adsorption, to further support cell adhesion (Figure 3a). The villi-wells were seeded with Caco-2 cells, a well-

established model cell line that upon differentiation exhibits characteristics similar to the native intestinal enterocytes.[4,5] Live staining (calcein-AM) after three weeks of culture, the standard period for Caco-2 cells to differentiate in 2D culture systems, revealed a confluent monolayer in all villi-wells (Figure 3c,d). Equivalent results were found using culture of Caco-2 cells at different passage numbers (Figure S5a). Dead staining showed a higher number of dead cells in villi-wells with the narrowest interpillar spacing (60 µm) (Figure S5b). The cause is likely stronger oxygen depletion at the well bottom due to a higher effective seeding density, since the same number of cells were seeded in all wells and villi-wells with a 60-µm interpillar spacing have the smallest surface area between the pillars to accommodate the sedimenting cells just after seeding (Table S1).

Monolithic dual-material villi-well devices enable facile barrier integrity assessment

Intestinal barrier models for compound screening should ideally allow for easy quantification of the barrier integrity. Most reported 3D hydrogel scaffolds mimicking the villus-crypt topography require substantial efforts to perform transport studies, since dissolved species can not only be transported through the cultured epithelial layer but also through the surrounding diffusion-open hydrogel material. Our dual compartment system overcomes this problem and enables simple TEER analysis and barrier integrity studies.

Formation of a functional barrier can be monitored by TEER measurement using the setup illustrated in Figure 4a. The experiment was conducted for the villi-wells of varied inter-pillar spacing as well as the flat-bottom system (Figure 4b). TEER values for Caco-2 cell layers cultured on hydrogel scaffolds were generally found to be lower than those cultured directly on the

polycarbonate membrane in Transwells as control (Figure S6a), in agreement with previous reports.[27,29,35,44] This can be explained by distinctly different mechanical properties of the hydrogels, coupled with the effect of the surface topography in villi-wells. The temporal development of the TEER shows a sigmoidal behavior in the villi-wells, which could be interpreted as cells gradually moving onto the micropillars and covering their surfaces (Figure 4b). However, immunofluorescence imaging of cell nuclei and of the tight junction protein zonula occludens-1 (ZO-1) in cell layers cultured for 10 and 21 days reveal that the micropillars are already populated on day 10, while tight junctions only developed over longer culture times (Figure S7b and 5a). The sharp increase in TEER around day 27 may indicate that the formed barrier tissue started to mature in terms of cellular differentiation and polarization, which reached full development after 45 days. A faster sigmoidal development in TEER values is observed in flat-bottomed wells (Figure 4b), possibly due to the smaller developed surface area to be covered by cells prior to tight junction formation.

The barrier function of the villi-well models was assessed by introducing a fluorescent probe (4.4 kDa TRITC-dextran) on the apical side (inside the well) followed by the measurement of the fluorescence intensity in the basal volume. Villi-wells without seeded cells were used as controls. The results in Figure 4c for the control villi-wells show little difference in probe retention compared to control experiments using a Transwell only (Figure S6b), confirming that the printed hydrogel bottom is nearly fully diffusion-open to compounds of this molar weight. In contrast, when an intact, tight barrier is formed by the epithelial cell layer on the hydrogel compartment, the fluorescent probe is largely retained in the villi-wells (note the gap in the intensity scale). Induced disruption of the formed barrier was investigated by addition of 100 µM staurosporine, an inducer of apoptosis,[35] to the apical volume. This yielded a higher signal in the basal medium,

and the barrier integrity was found to gradually diminish over time (Figure 4d). Interestingly, cells cultured in printed flat-bottom wells showed much smaller difference in barrier integrity on drug-induced disruption. Similarly, conventional Transwell systems have also been reported to exhibit much lower changes in barrier disruption assessment.[35] These observations collectively supports that the topographical features of the villi-wells — and not only the hydrogel substrate — leads to an improved 3D barrier model compared to Transwells and 2D cultures.

Printed pillar materials optimized for cell adhesion support apico-basal polarization and tight-junction formation

Figure 5 shows 3D reconstructions of two-photon fluorescence micrographs of the villi-wells after 45 days of culture, when the cell layer has fully developed into a tight and functional barrier according to the TEER measurement. The confluent Caco-2 cell layers expressed tight junction markers (ZO-1) between cells (Figure 5a and S5b) and apical localization of brush-border specific Ezrin indicating brush border formation and polarization of the cells (Figure 5b and S5c). These markers were expressed at all elevations of the micropillars for interpillar spacings of 120 μm and 180 μm, with a decreased observed intensity towards the pillar bottom. The lower intensity is likely caused by limited optical access but may also be due to differences in differentiation behavior by the incorporated 3D microarchitectures along the crypt-villus axis, with cells being less differentiated towards the bottom.[23,29] Orthographic projections of the pillar sides (Figure 5b) clearly show that cell nuclei are oriented closer to the underlying surface (basal nuclei), while Ezrin covers the apical side in agreement with the formation of a polarized epithelium. The micrographs also show that the villi-like micropillars maintained their structural integrity over a

long culture period (up to 45 days), which indicates that our proposed approach is suitable for long-term *in vitro* studies due to the minimal degradation and post-printing swelling of our developed hydrogel material. For the villi-wells of narrowest inter-pillar spacing (60 μm) cell clusters accumulated between neighboring pillars, which strongly decreased the observable intensity towards the bottom and made the imaged pillars appear lower than their true height (cf. Figure 2c). We note that cell coverage of the printed villi-like micropillars as well as tight junction formation was noticeable already within a 10-day culture period, while brush border formation was only observed after a 3-week culture period (Figure 5b and S5c). These results collectively suggest that our 3D printed villi-like scaffolds support gradual cellular growth, differentiation, and polarization of intestinal enterocytes.

Conclusions

We have developed a fast and simple dual-material stereolithographic 3D printing modality, which enables the manufacture of monolithic transport analysis devices mimicking important topographical properties of small intestinal tissue and permitting quantitative data acquisition, to narrow the gap between simpler commonly used intestinal barrier models and the native tissue. Thanks to the high resolution and high reproducibility of SLA 3D printing, micropillars of anatomically relevant shapes were printed with tunable density at the bottom of the two-material villi-wells having a well-defined interface, and the micropillars were found to influence the growth pattern (time to barrier formation) and barrier properties (TEER) of the resulting barrier model. Our method combines different macromers with matching cross-linking chemistries in separate printing sequence steps to manufacture cytocompatible polymeric constructs with different

physiochemical properties integrated in a monolithic device. In future work, we will leverage SLA's demonstrated ability (by us and others) of manufacturing complex microfluidic devices[54,59] to extend our presented approach with additional material layers for engineering next-generation *in vitro* intestinal models that capture both essential structural and dynamic *in vivo* cues.

ASSOCIATED CONTENT

Supporting Information.

The Supporting Information is available free of charge at https://pubs.acs.org/doi/10.1021/acsami.xxxx.

Mechanical analysis of the printed materials; Optimization of the 3D printing of PEGDA250; Cytotoxicity analysis of printed material; Cohesion analysis of sequentially printed materials; Optical characterization of printed micropillar arrays; Cell coverage visualization; TEER and fluorescent tracer control experiments; Tight junction and polarization visualization; Villi-well / Transwell compatibility. (PDF)

AUTHOR INFORMATION

Corresponding Authors

* Thomas L. Andresen — Center for Intestinal Absorption and Transport of Biopharmaceuticals, Department of Health Technology, Technical University of Denmark, DK-2800, Kgs. Lyngby, Denmark; orcid.org/0000-0002-1048-127X; Email: tlan@dtu.dk

* Niels B. Larsen — Center for Intestinal Absorption and Transport of Biopharmaceuticals, Department of Health Technology, Technical University of Denmark, DK-2800, Kgs. Lyngby, Denmark; orcid.org/0000-0001-6506-3991; Email: nibl@dtu.dk

Authors

Nayere Taebnia — Center for Intestinal Absorption and Transport of Biopharmaceuticals, Department of Health Technology, Technical University of Denmark, DK-2800, Kgs. Lyngby, Denmark; orcid.org/0000-0003-0707-278X

Rujing Zhang — Center for Intestinal Absorption and Transport of Biopharmaceuticals, Department of Health Technology, Technical University of Denmark, DK-2800, Kgs. Lyngby, Denmark; orcid.org/0000-0002-0029-848X

Emil B. Kromann — Center for Intestinal Absorption and Transport of Biopharmaceuticals, Department of Health Technology, Technical University of Denmark, DK-2800, Kgs. Lyngby, Denmark; orcid.org/0000-0002-0782-1624

Alireza Dolatshahi-Pirouz — Center for Intestinal Absorption and Transport of Biopharmaceuticals, Department of Health Technology, Technical University of Denmark, DK-2800, Kgs. Lyngby, Denmark; orcid.org/0000-0001-6326-0836

Author Contributions

‡N.T. and R.Z. contributed equally to this work.

Funding Sources

This work was supported by the Novo Nordisk Foundation (Grant No NNF16OC0022166).

Notes

The authors declare no competing financial interest.

REFERENCES

(1) Lundquist, P.; Artursson, P. Oral Absorption of Peptides and Nanoparticles across the Human Intestine: Opportunities, Limitations and Studies in Human Tissues. *Adv. Drug Deliv. Rev.* **2016**, *106*, 256–276. https://doi.org/10.1016/j.addr.2016.07.007.

(2) Yu, J.; Carrier, R. L.; March, J. C.; Griffith, L. G. Three Dimensional Human Small Intestine Models for ADME-Tox Studies. *Drug Discov. Today* **2014**, *19* (10), 1587–1594. https://doi.org/10.1016/j.drudis.2014.05.003.

(3) Larsen, J. B.; Taebnia, N.; Dolatshahi-Pirouz, A.; Eriksen, A. Z.; Hjørringgaard, C.; Kristensen, K.; Larsen, N. W.; Larsen, N. B.; Marie, R.; Mündler, A.-K.; et al. Imaging Therapeutic Peptide Transport across Intestinal Barriers. *RSC Chem. Biol.* **2021**. https://doi.org/10.1039/d1cb00024a.

(4) Artursson, P.; Palm, K.; Luthman, K. Caco-2 Monolayers in Experimental and Theoretical Predictions of Drug Transport. *Adv. Drug Deliv. Rev.* **2012**, *64* (SUPPL.), 280–289. https://doi.org/10.1016/j.addr.2012.09.005.

(5) Sambuy, Y.; De Angelis, I.; Ranaldi, G.; Scarino, M. L.; Stammati, A.; Zucco, F. The Caco-2 Cell Line as a Model of the Intestinal Barrier: Influence of Cell and Culture-Related Factors on Caco-2 Cell Functional Characteristics. *Cell Biol. Toxicol.* **2005**, *21* (1), 1–26. https://doi.org/10.1007/s10565-005-0085-6.

(6) Abbott, A. Biology's New Dimension. *Nature* **2003**, *424* (6951), 870–872.

https://doi.org/10.1038/424870a.

(7) Barker, N. Adult Intestinal Stem Cells: Critical Drivers of Epithelial Homeostasis and Regeneration. *Nat. Rev. Mol. Cell Biol.* **2014**, *15* (1), 19–33. https://doi.org/10.1038/nrm3721.

(8) Kelly, P.; Menzies, I.; Crane, R.; Zulu, I.; Nickols, C.; Feakins, R.; Mwansa, J.; Mudenda, V.; Katubulushi, M.; Greenwald, S.; et al. Responses of Small Intestinal Architecture and Function over Time to Environmental Factors in a Tropical Population. *Am. J. Trop. Med. Hyg.* **2004**, *70* (4), 412–419. https://doi.org/10.4269/ajtmh.2004.70.412.

(9) Bein, A.; Shin, W.; Jalili-Firoozinezhad, S.; Park, M. H.; Sontheimer-Phelps, A.; Tovaglieri, A.; Chalkiadaki, A.; Kim, H. J.; Ingber, D. E. Microfluidic Organ-on-a-Chip Models of Human Intestine. *Cell. Mol. Gastroenterol. Hepatol.* **2018**, *5* (4), 659–668. https://doi.org/10.1016/j.jcmgh.2017.12.010.

(10) Dosh, R. H.; Jordan-Mahy, N.; Sammon, C.; Le Maitre, C. L. Tissue Engineering Laboratory Models of the Small Intestine. *Tissue Eng. Part B Rev.* **2018**, *24* (2), 98–111. https://doi.org/10.1089/ten.teb.2017.0276.

(11) Barrila, J.; Radtke, A. L.; Crabbé, A.; Sarker, S. F.; Herbst-Kralovetz, M. M.; Ott, C. M.; Nickerson, C. A. Organotypic 3D Cell Culture Models: Using the Rotating Wall Vessel to Study Host-Pathogen Interactions. *Nat. Rev. Microbiol.* **2010**, *8* (11), 791–801. https://doi.org/10.1038/nrmicro2423.

(12) Sato, T.; Vries, R. G.; Snippert, H. J.; van de Wetering, M.; Barker, N.; Stange, D. E.; van Es, J. H.; Abo, A.; Kujala, P.; Peters, P. J.; et al. Single Lgr5 Stem Cells Build Crypt-Villus

Structures in Vitro without a Mesenchymal Niche. *Nature* **2009**, *459* (7244), 262–265. https://doi.org/10.1038/nature07935.

(13) Cruz-Acuña, R.; Quirós, M.; Farkas, A. E.; Dedhia, P. H.; Huang, S.; Siuda, D.; García-Hernández, V.; Miller, A. J.; Spence, J. R.; Nusrat, A.; et al. Synthetic Hydrogels for Human Intestinal Organoid Generation and Colonic Wound Repair. *Nat. Cell Biol.* **2017**, *19* (11), 1326–1335. https://doi.org/10.1038/ncb3632.

(14) Sachs, N.; Tsukamoto, Y.; Kujala, P.; Peters, P. J.; Clevers, H. Intestinal Epithelial Organoids Fuse to Form Self-Organizing Tubes in Floating Collagen Gels. *Dev.* **2017**, *144* (6), 1107–1112. https://doi.org/10.1242/dev.143933.

(15) Sung, J. H.; Yu, J.; Luo, D.; Shuler, M. L.; March, J. C. Microscale 3-D Hydrogel Scaffold for Biomimetic Gastrointestinal (GI) Tract Model. *Lab Chip* **2011**, *11* (3), 389–392. https://doi.org/10.1039/C0LC00273A.

(16) Yu, J.; Peng, S.; Luo, D.; March, J. C. In Vitro 3D Human Small Intestinal Villous Model for Drug Permeability Determination. *Biotechnol. Bioeng.* **2012**, *109* (9), 2173–2178. https://doi.org/10.1002/bit.24518.

(17) Yi, B.; Shim, K. Y.; Ha, S. K.; Han, J.; Hoang, H.-H.; Choi, I.; Park, S.; Sung, J. H. Three-Dimensional in Vitro Gut Model on a Villi-Shaped Collagen Scaffold. *BioChip J.* **2017**, *11* (3), 219–231. https://doi.org/10.1007/s13206-017-1307-8.

(18) Wang, Y.; Kim, R.; Gunasekara, D. B.; Reed, M. I.; DiSalvo, M.; Nguyen, D. L.; Bultman, S. J.; Sims, C. E.; Magness, S. T.; Allbritton, N. L. Formation of Human Colonic Crypt Array by Application of Chemical Gradients Across a Shaped Epithelial Monolayer. *Cmgh*

2018, *5* (2), 113–130. https://doi.org/10.1016/j.jcmgh.2017.10.007.

(19) Castaño, A. G.; García-Díaz, M.; Torras, N.; Altay, G.; Comelles, J.; Martínez, E. Dynamic Photopolymerization Produces Complex Microstructures on Hydrogels in a Moldless Approach to Generate a 3D Intestinal Tissue Model. *Biofabrication* **2019**, *11* (2), 025007. https://doi.org/10.1088/1758-5090/ab0478.

(20) Wang, L.; Murthy, S. K.; Fowle, W. H.; Barabino, G. A.; Carrier, R. L. Influence of Micro-Well Biomimetic Topography on Intestinal Epithelial Caco-2 Cell Phenotype. *Biomaterials* **2009**, *30* (36), 6825–6834. https://doi.org/10.1016/j.biomaterials.2009.08.046.

(21) Wang, L.; Murthy, S. K.; Barabino, G. A.; Carrier, R. L. Synergic Effects of Crypt-like Topography and ECM Proteins on Intestinal Cell Behavior in Collagen Based Membranes. *Biomaterials* **2010**, *31* (29), 7586–7598. https://doi.org/10.1016/j.biomaterials.2010.06.036.

(22) Esch, M. B.; Sung, J. H.; Yang, J.; Yu, C.; Yu, J.; March, J. C.; Shuler, M. L. On Chip Porous Polymer Membranes for Integration of Gastrointestinal Tract Epithelium with Microfluidic 'Body-on-a-Chip' Devices. *Biomed. Microdevices* **2012**, *14* (5), 895–906. https://doi.org/10.1007/s10544-012-9669-0.

(23) Costello, C. M.; Hongpeng, J.; Shaffiey, S.; Yu, J.; Jain, N. K.; Hackam, D.; March, J. C. Synthetic Small Intestinal Scaffolds for Improved Studies of Intestinal Differentiation. *Biotechnol. Bioeng.* **2014**, *111* (6), 1222–1232. https://doi.org/10.1002/bit.25180.

(24) Kim, S. H.; Chi, M.; Yi, B.; Kim, S. H.; Oh, S.; Kim, Y.; Park, S.; Sung, J. H. Three-Dimensional Intestinal Villi Epithelium Enhances Protection of Human Intestinal Cells

from Bacterial Infection by Inducing Mucin Expression. *Integr. Biol.* **2014**, *6* (12), 1122–1131. https://doi.org/10.1039/c4ib00157e.

(25) Costello, C. M.; Sorna, R. M.; Goh, Y.-L.; Cengic, I.; Jain, N. K.; March, J. C. 3-D Intestinal Scaffolds for Evaluating the Therapeutic Potential of Probiotics. *Mol. Pharm.* **2014**, *11* (7), 2030–2039. https://doi.org/10.1021/mp5001422.

(26) Chen, Y.; Lin, Y.; Davis, K. M.; Wang, Q.; Rnjak-Kovacina, J.; Li, C.; Isberg, R. R.; Kumamoto, C. A.; Mecsas, J.; Kaplan, D. L. Robust Bioengineered 3D Functional Human Intestinal Epithelium. *Sci. Rep.* **2015**, *5* (1), 13708. https://doi.org/10.1038/srep13708.

(27) Koppes, A. N.; Kamath, M.; Pfluger, C. A.; Burkey, D. D.; Dokmeci, M.; Wang, L.; Carrier, R. L. Complex, Multi-Scale Small Intestinal Topography Replicated in Cellular Growth Substrates Fabricated via Chemical Vapor Deposition of Parylene C. *Biofabrication* **2016**, *8* (3), 035011. https://doi.org/10.1088/1758-5090/8/3/035011.

(28) Shaffiey, S. A.; Jia, H.; Keane, T.; Costello, C.; Wasserman, D.; Quidgley, M.; Dziki, J.; Badylak, S.; Sodhi, C. P.; March, J. C.; et al. Intestinal Stem Cell Growth and Differentiation on a Tubular Scaffold with Evaluation in Small and Large Animals. *Regen. Med.* **2016**, *11* (1), 45–61. https://doi.org/10.2217/rme.15.70.

(29) Wang, Y.; Gunasekara, D. B.; Reed, M. I.; DiSalvo, M.; Bultman, S. J.; Sims, C. E.; Magness, S. T.; Allbritton, N. L. A Microengineered Collagen Scaffold for Generating a Polarized Crypt-Villus Architecture of Human Small Intestinal Epithelium. *Biomaterials* **2017**, *128*, 44–55. https://doi.org/10.1016/j.biomaterials.2017.03.005.

(30) Srinivasan, B.; Kolli, A. R.; Esch, M. B.; Abaci, H. E.; Shuler, M. L.; Hickman, J. J. TEER

Measurement Techniques for In Vitro Barrier Model Systems. *J. Lab. Autom.* **2015**, *20* (2), 107–126. https://doi.org/10.1177/2211068214561025.

(31) Kimura, H.; Yamamoto, T.; Sakai, H.; Sakai, Y.; Fujii, T. An Integrated Microfluidic System for Long-Term Perfusion Culture and on-Line Monitoring of Intestinal Tissue Models. *Lab Chip* **2008**, *8* (5), 741. https://doi.org/10.1039/b717091b.

(32) Kim, H. J.; Huh, D.; Hamilton, G.; Ingber, D. E. Human Gut-on-a-Chip Inhabited by Microbial Flora That Experiences Intestinal Peristalsis-like Motions and Flow. *Lab Chip* **2012**, *12* (12), 2165. https://doi.org/10.1039/c2lc40074j.

(33) Kim, H. J.; Ingber, D. E. Gut-on-a-Chip Microenvironment Induces Human Intestinal Cells to Undergo Villus Differentiation. *Integr. Biol. (United Kingdom)* **2013**, *5* (9), 1130–1140. https://doi.org/10.1039/c3ib40126j.

(34) Kim, H. J.; Li, H.; Collins, J. J.; Ingber, D. E. Contributions of Microbiome and Mechanical Deformation to Intestinal Bacterial Overgrowth and Inflammation in a Human Gut-on-a-Chip. *Proc. Natl. Acad. Sci.* **2016**, *113* (1), E7–E15. https://doi.org/10.1073/pnas.1522193112.

(35) Trietsch, S. J.; Naumovska, E.; Kurek, D.; Setyawati, M. C.; Vormann, M. K.; Wilschut, K. J.; Lanz, H. L.; Nicolas, A.; Ng, C. P.; Joore, J.; et al. Membrane-Free Culture and Real-Time Barrier Integrity Assessment of Perfused Intestinal Epithelium Tubes. *Nat. Commun.* **2017**, *8* (1), 262. https://doi.org/10.1038/s41467-017-00259-3.

(36) Kasendra, M.; Tovaglieri, A.; Sontheimer-Phelps, A.; Jalili-Firoozinezhad, S.; Bein, A.; Chalkiadaki, A.; Scholl, W.; Zhang, C.; Rickner, H.; Richmond, C. A.; et al. Development

of a Primary Human Small Intestine-on-a-Chip Using Biopsy-Derived Organoids. *Sci. Rep.* **2018**, *8* (1), 2871. https://doi.org/10.1038/s41598-018-21201-7.

(37) Workman, M. J.; Gleeson, J. P.; Troisi, E. J.; Estrada, H. Q.; Kerns, S. J.; Hinojosa, C. D.; Hamilton, G. A.; Targan, S. R.; Svendsen, C. N.; Barrett, R. J. Enhanced Utilization of Induced Pluripotent Stem Cell–Derived Human Intestinal Organoids Using Microengineered Chips. *Cell. Mol. Gastroenterol. Hepatol.* **2018**, *5* (4), 669-677.e2. https://doi.org/10.1016/j.jcmgh.2017.12.008.

(38) Delon, L. C.; Guo, Z.; Oszmiana, A.; Chien, C.-C.; Gibson, R.; Prestidge, C.; Thierry, B. A Systematic Investigation of the Effect of the Fluid Shear Stress on Caco-2 Cells towards the Optimization of Epithelial Organ-on-Chip Models. *Biomaterials* **2019**, *225* (September), 119521. https://doi.org/10.1016/j.biomaterials.2019.119521.

(39) Nikolaev, M.; Mitrofanova, O.; Broguiere, N.; Geraldo, S.; Dutta, D.; Tabata, Y.; Elci, B.; Brandenberg, N.; Kolotuev, I.; Gjorevski, N.; et al. Homeostatic Mini-Intestines through Scaffold-Guided Organoid Morphogenesis. *Nature* **2020**, *585* (7826), 574–578. https://doi.org/10.1038/s41586-020-2724-8.

(40) Ramadan, Q.; Jafarpoorchekab, H.; Huang, C.; Silacci, P.; Carrara, S.; Koklü, G.; Ghaye, J.; Ramsden, J.; Ruffert, C.; Vergeres, G.; et al. NutriChip: Nutrition Analysis Meets Microfluidics. *Lab Chip* **2013**, *13* (2), 196–203. https://doi.org/10.1039/C2LC40845G.

(41) Chi, M.; Yi, B.; Oh, S.; Park, D. J.; Sung, J. H.; Park, S. A Microfluidic Cell Culture Device (MFCCD) to Culture Epithelial Cells with Physiological and Morphological Properties That Mimic Those of the Human Intestine. *Biomed. Microdevices* **2015**, *17* (3), 1–10. https://doi.org/10.1007/s10544-015-9966-5.

(42) Henry, O. Y. F.; Villenave, R.; Cronce, M. J.; Leineweber, W. D.; Benz, M. A.; Ingber, D. E. Organs-on-Chips with Integrated Electrodes for Trans-Epithelial Electrical Resistance (TEER) Measurements of Human Epithelial Barrier Function. *Lab Chip* **2017**, *17* (13), 2264–2271. https://doi.org/10.1039/c7lc00155j.

(43) Waheed, S.; Cabot, J. M.; Macdonald, N. P.; Lewis, T.; Guijt, R. M.; Paull, B.; Breadmore, M. C. 3D Printed Microfluidic Devices: Enablers and Barriers. *Lab Chip* **2016**, *16* (11), 1993–2013. https://doi.org/10.1039/C6LC00284F.

(44) Creff, J.; Courson, R.; Mangeat, T.; Foncy, J.; Souleille, S.; Thibault, C.; Besson, A.; Malaquin, L. Fabrication of 3D Scaffolds Reproducing Intestinal Epithelium Topography by High-Resolution 3D Stereolithography. *Biomaterials* **2019**, *221* (August), 119404. https://doi.org/10.1016/j.biomaterials.2019.119404.

(45) Melchels, F. P. W.; Feijen, J.; Grijpma, D. W. A Review on Stereolithography and Its Applications in Biomedical Engineering. *Biomaterials* **2010**, *31* (24), 6121–6130. https://doi.org/10.1016/j.biomaterials.2010.04.050.

(46) Billiet, T.; Vandenhaute, M.; Schelfhout, J.; Van Vlierberghe, S.; Dubruel, P. A Review of Trends and Limitations in Hydrogel-Rapid Prototyping for Tissue Engineering. *Biomaterials* **2012**, *33* (26), 6020–6041. https://doi.org/10.1016/j.biomaterials.2012.04.050.

(47) Lu, Y.; Mapili, G.; Suhali, G.; Chen, S.; Roy, K. A Digital Micro-Mirror Device-Based System for the Microfabrication of Complex, Spatially Patterned Tissue Engineering Scaffolds. *J. Biomed. Mater. Res. - Part A* **2006**, *77* (2), 396–405. https://doi.org/10.1002/jbm.a.30601.

(48) Han, L. H.; Suri, S.; Schmidt, C. E.; Chen, S. Fabrication of Three-Dimensional Scaffolds for Heterogeneous Tissue Engineering. *Biomed. Microdevices* **2010**, *12* (4), 721–725. https://doi.org/10.1007/s10544-010-9425-2.

(49) Arcaute, K.; Mann, B. K.; Wicker, R. B. Stereolithography of Three-Dimensional Bioactive Poly(Ethylene Glycol) Constructs with Encapsulated Cells. *Ann. Biomed. Eng.* **2006**, *34* (9), 1429–1441. https://doi.org/10.1007/s10439-006-9156-y.

(50) Chan, V.; Zorlutuna, P.; Jeong, J. H.; Kong, H.; Bashir, R. Three-Dimensional Photopatterning of Hydrogels Using Stereolithography for Long-Term Cell Encapsulation. *Lab Chip* **2010**, *10* (16), 2062–2070. https://doi.org/10.1039/c004285d.

(51) Ma, X.; Qu, X.; Zhu, W.; Li, Y.-S.; Yuan, S.; Zhang, H.; Liu, J.; Wang, P.; Lai, C. S. E.; Zanella, F.; et al. Deterministically Patterned Biomimetic Human IPSC-Derived Hepatic Model via Rapid 3D Bioprinting. *Proc. Natl. Acad. Sci.* **2016**, *113* (8), 201524510. https://doi.org/10.1073/pnas.1524510113.

(52) Kim, Y. T.; Castro, K.; Bhattacharjee, N.; Folch, A. Digital Manufacturing of Selective Porous Barriers in Microchannels Using Multi-Material Stereolithography. *Micromachines* **2018**, *9* (3). https://doi.org/10.3390/mi9030125.

(53) Van Den Bulcke, A. I.; Bogdanov, B.; De Rooze, N.; Schacht, E. H.; Cornelissen, M.; Berghmans, H. Structural and Rheological Properties of Methacrylamide Modified Gelatin Hydrogels. *Biomacromolecules* **2000**, *1* (1), 31–38. https://doi.org/10.1021/bm990017d.

(54) Zhang, R.; Larsen, N. B. Stereolithographic Hydrogel Printing of 3D Culture Chips with Biofunctionalized Complex 3D Perfusion Networks. *Lab Chip* **2017**, *17* (24), 4273–4282.

https://doi.org/10.1039/c7lc00926g.

(55) Christensen, R. K.; Von Halling Laier, C.; Kiziltay, A.; Wilson, S.; Larsen, N. B. 3D Printed Hydrogel Multiassay Platforms for Robust Generation of Engineered Contractile Tissues. *Biomacromolecules* **2020**, *21* (2), 356–365. https://doi.org/10.1021/acs.biomac.9b01274.

(56) Treloar, L. R. G. *The Physics of Rubber Elasticity*, 3rd ed.; Oxford University Press, 1975.

(57) Rosenegger, D. G.; Tran, C. H. T.; LeDue, J.; Zhou, N.; Gordon, G. R. A High Performance, Cost-Effective, Open-Source Microscope for Scanning Two-Photon Microscopy That Is Modular and Readily Adaptable. *PLoS One* **2014**, *9* (10), e110475. https://doi.org/10.1371/journal.pone.0110475.

(58) Zhu, J. Bioactive Modification of Poly(Ethylene Glycol) Hydrogels for Tissue Engineering. *Biomaterials* **2010**, *31* (17), 4639–4656. https://doi.org/10.1016/j.biomaterials.2010.02.044.

(59) Gong, H.; Bickham, B. P.; Woolley, A. T.; Nordin, G. P. Custom 3D Printer and Resin for 18 Mm × 20 Mm Microfluidic Flow Channels. *Lab Chip* **2017**, *17* (17), 2899–2909. https://doi.org/10.1039/C7LC00644F.

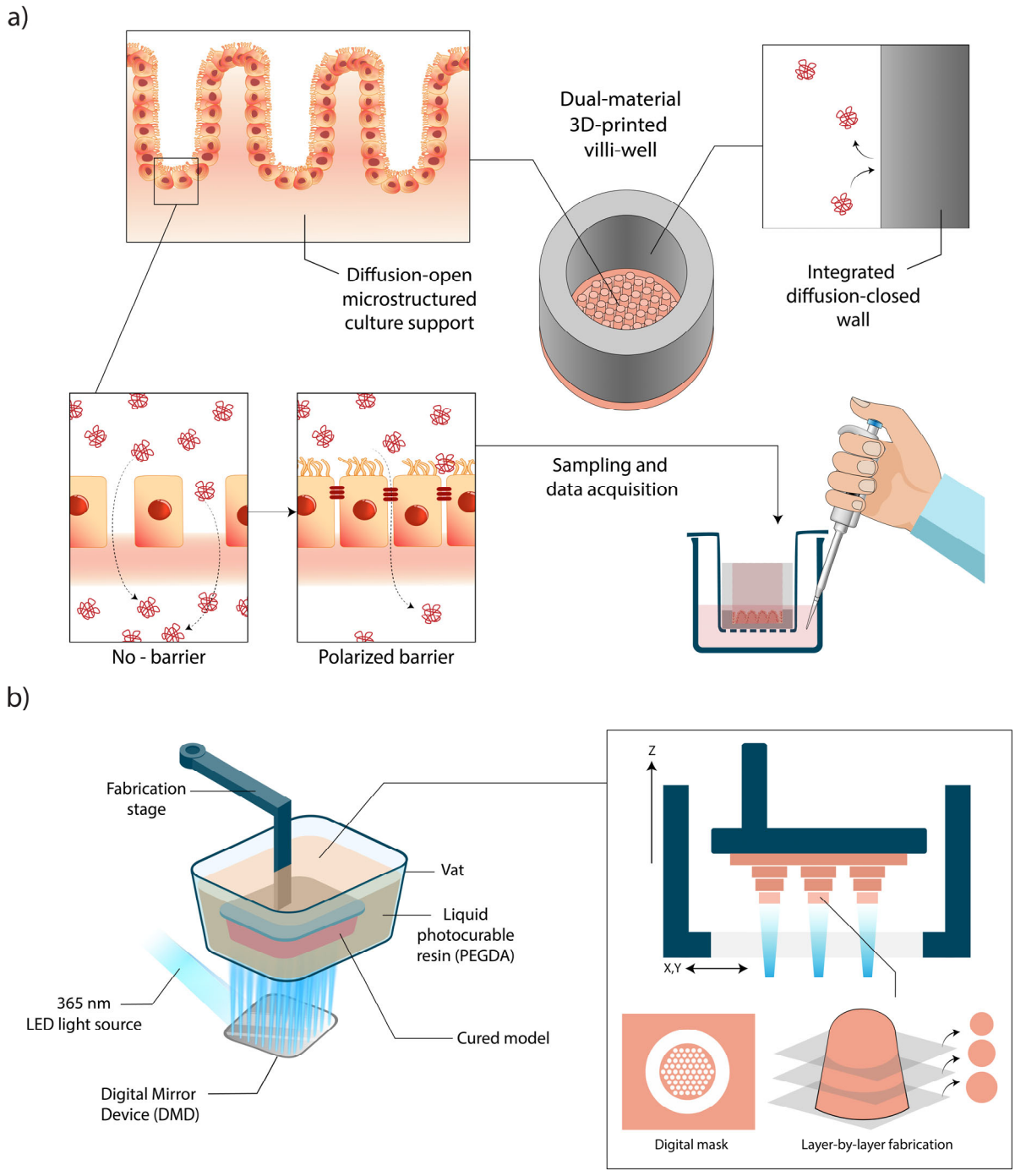

Scheme 1. Engineering monolithic transport analysis devices with villi-like surface microstructures using dual-material stereolithography. a) Illustration of a 3D dual-material printed villi-well with a printed hydrogel bottom featuring villi-like microstructures. The hydrogel bottom supports diffusion of biological molecules and culture of intestinal epithelium, while the

surrounding wall printed in a non-permeable material restricts mass transport to the formed cellular barrier lining device bottom. b) The monolithic devices are produced by stereolithographic high-resolution 3D printing in a vat sequentially containing one of two photo-crosslinkable poly(ethylene glycol)-diacrylate (PEGDA)-based resins to manufacture diffusion-open or diffusion-closed final materials.

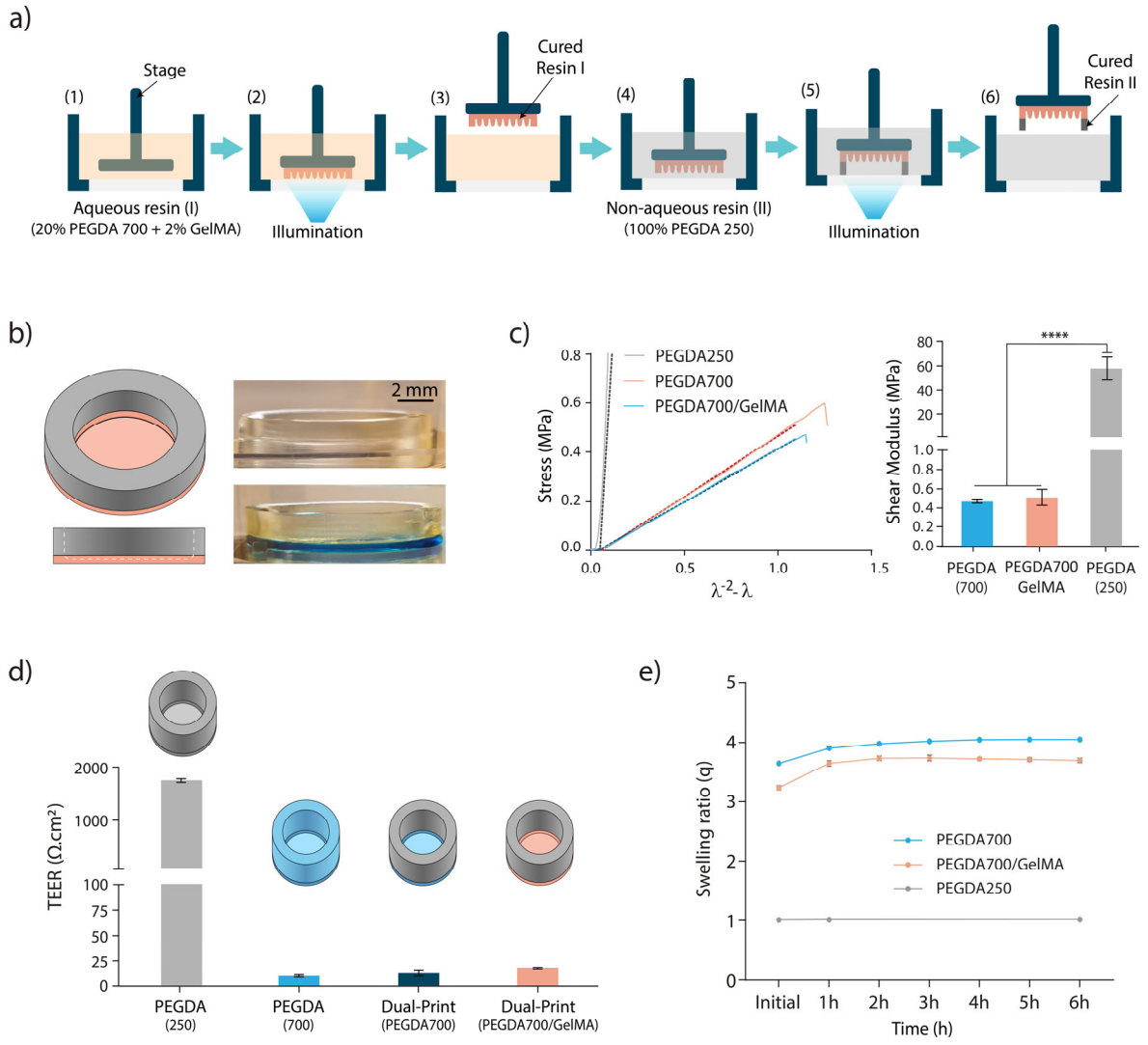

Figure 1. Characterization of the dual material printed structures. a) The bottom of villi-wells is printed using resin I (20% PEGDA700/2% GelMA) shown in pink, followed by printing the diffusion-closed walls made of resin II (100% PEGDA250) shown in gray. b) Illustration of a flat-bottom dual-material well and side view photographs of an all-PEGDA250 print (top) and a dual-material print (bottom) after 2 h of incubation with an aqueous blue food dye solution. c) Uniaxial compression of 3D printed solid cylinders of different resin formulations. The measured stress (solid lines) is displayed versus $\lambda^{-2} - \lambda$ (neo-Hookean elastic theory), where λ is the extension

ratio. The shear modulus is obtained by linear fitting (dashed lines). d) Transepithelial electric resistance (TEER) analysis on cell-free 3D printed wells confirms that PEGDA250 prints are diffusion-closed to ions in aqueous media. e) Time-dependent mass swelling ratio of 3D printed solid objects immersed in water shows that PEGDA250 exhibits minimal post-printing swelling, while PEGDA700-based materials show ~10% post-printing swelling.

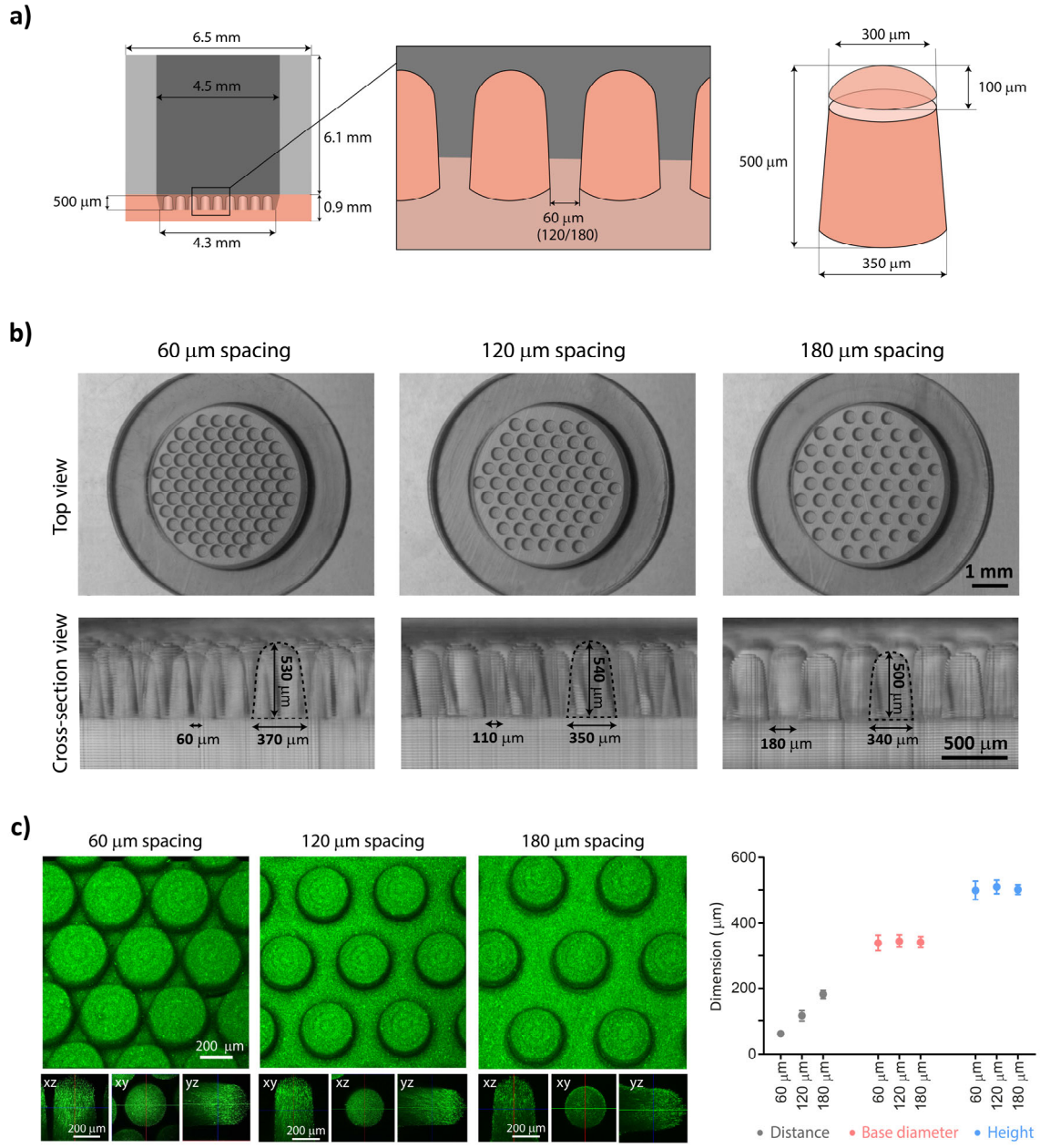

Figure 2. Microstructural design elements are faithfully reproduced in the 3D printed villi-wells. a) Schematic cross-section of the dual-material villi-wells with varied interpillar distances, presenting a culture support mimicking the topography and dimensions of human small intestinal epithelium. b) Optical micrographs showing top views (upper row) and cross-sectional view (lower row) of printed villi-wells. The dashed line marks the boundary of a single villus-like micropillar.

Printed villi-wells were immersed in water overnight prior to imaging. c) (left) 3D reconstruction of confocal laser scanning micrographs (upper row of sub-panels) showing the printed villi-like micropillars, and cross-sectional views (xz, xy and yz; right) of a single micropillar visualized by two-photon fluorescence microscopy (lower row of sub-panels). (right) Analysis of the dimensional variations in the printed villi structures (error bars show the standard deviation) based on tiled confocal microscopy stacks of entire villi wells. Fluorescent microbeads (green) were added to the resin formulation to assist visualization.

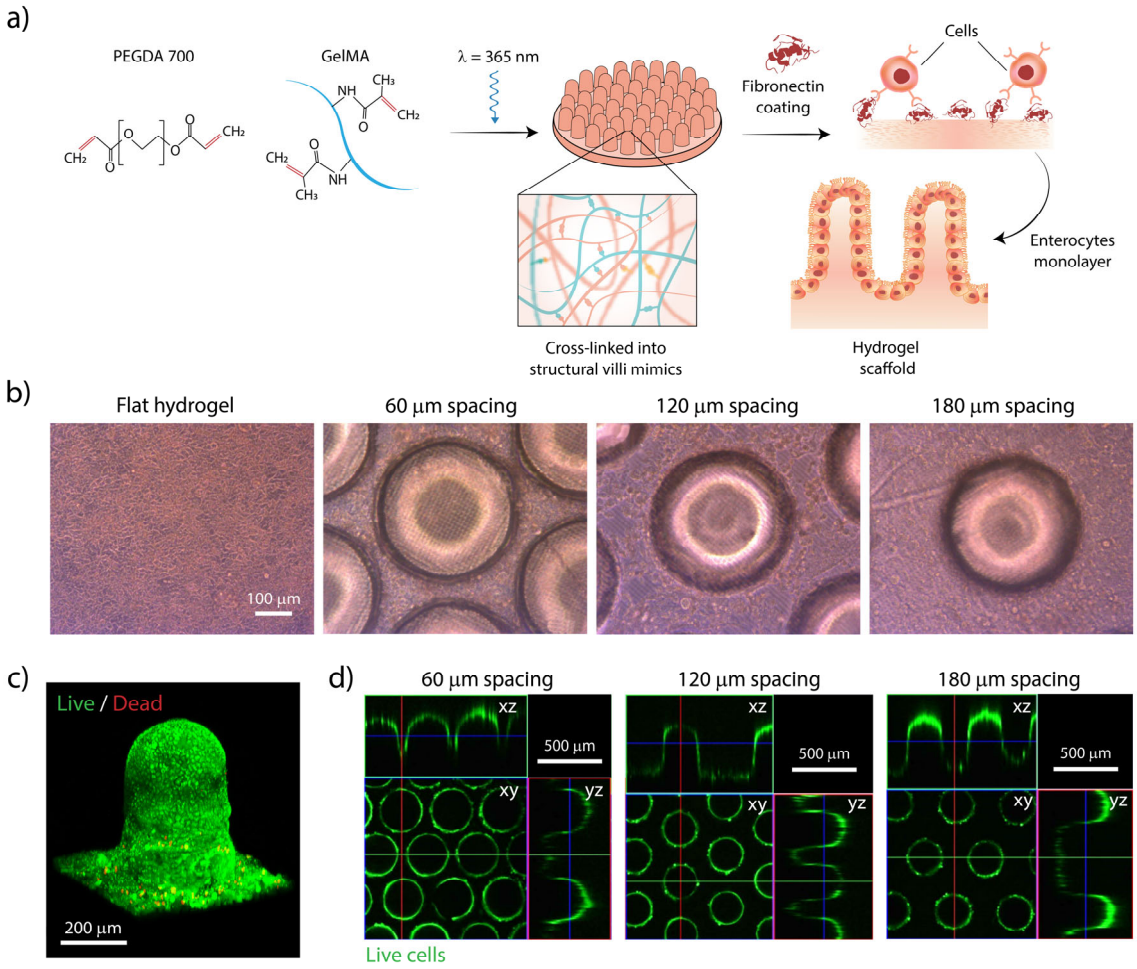

Figure 3. 3D printed hydrogel scaffolds are compatible with long-term dense enterocyte culture. a) The culture support is 3D printed by photochemical crosslinking of PEGDA 700 and GelMA to shape the hydrogel bottom of the villi-wells, followed by physical adsorption of fibronectin onto the 3D printed bottom to enhance enterocyte adhesion. The modified scaffolds are seeded with enterocytes to produce the intestinal tissue model. b) Representative phase-contrast images (top view) of human colon carcinoma cells (Caco-2) cultured for 21 days in 3D printed and fibronectin coated villi-wells of varied surface topography. c) Representative 3D reconstruction of two-photon fluorescence micrographs of individual villus-like micropillars covered with Caco-2 cells after 21 days of culture (live cells green, calcein AM; dead cells red, propidium iodide). d) Cross-sectional

views (xz, xy and yz) of live Caco-2 cells (calcein AM, green) cultured in villi-wells of varied inter-pillar spacing for 3 weeks and visualized by confocal laser scanning microscopy.

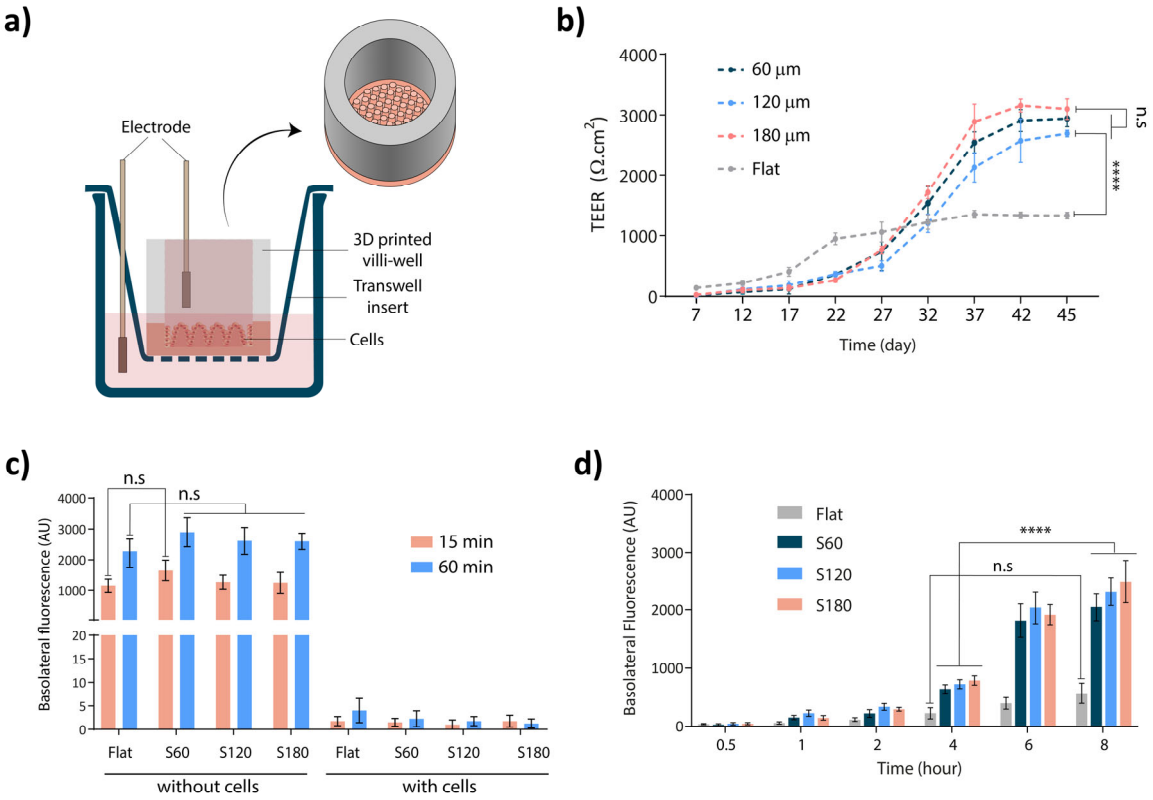

Figure 4. Villi-wells enable simple barrier integrity assessment. a) Schematic of a printed villi-well seeded with Caco-2 cells and the measurement setup used for both TEER and barrier integrity assays. b) Intestinal barrier function quantified by TEER measurement over time for Caco-2 cells cultured in villi-wells. c) Evaluation of the intestinal barrier function by introduction of 4.4 kDa TRITC-dextran into the villi-well (apical side) and measurement of the fluorescence intensity outside the Transwell insert (basolateral side) after 15 and 60 min. Villi-wells without cells were included as controls. d) Drug-induced loss of barrier integrity over time. The apical-side medium was replaced with a solution of TRITC-dextran supplemented with staurosporine, and basolateral medium was sampled for fluorescence analysis at the indicated time points.

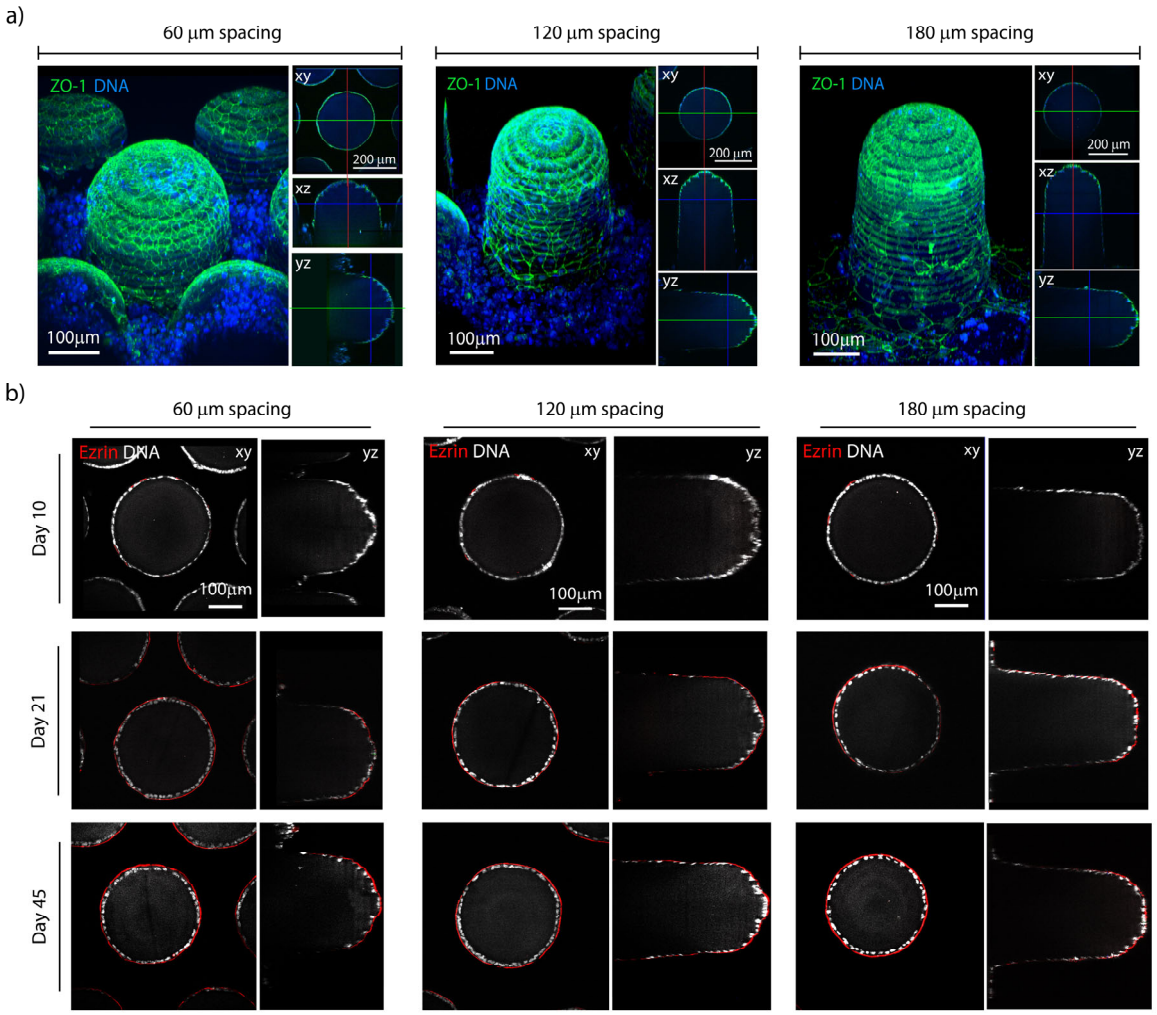

Figure 5. Villi-wells support apico-basal polarization of Caco-2 cells. Cells were seeded in 3D printed dual-material villi-wells and cultured for up to 45 days, followed by fixation and staining for nucleic acid (blue), ZO-1 (green) and Ezrin (red). a) 3D reconstruction of z-stack images (left) as well as cross-sectional views (xz, xy and yz; right) of Caco-2 cells cultured for 45 days in printed villi-wells by two-photon fluorescence microscopy, displaying tight junctions (stained for ZO-1) on the tip and over the vertical sides of the villi-like micropillars. b) Cross-sectional views (xy and yz) of Caco-2 cells cultured for 10, 21 and 45 days in villi-wells by two-photon fluorescence

microscopy shows gradual brush border formation (expression of Ezrin) on the apical side, in support of the formation of a polarized tissue.